Flexible Films Derived from Electrospun Carbon Nanofibers Incorporated with Co_3O_4 Hollow Nanoparticles as Self-Supported Electrodes for Electrochemical Capacitors

Fang Zhang, Changzhou Yuan, Jiajia Zhu, Jie Wang, Xiaogang Zhang, and Xiong Wen (David) Lou**

Flexible porous films are prepared from electrospun carbon nanofibers (CNFs) embedded with Co_3O_4 hollow nanoparticles (NPs) and are directly applied as self-supported electrodes for high-performance electrochemical capacitors. Uniform Co_3O_4 hollow NPs are well dispersed and/or embedded into each CNF with desirable electrical conductivity. These Co_3O_4-CNFs intercross each other and form 3D hierarchical porous hybrid films. Benefiting from intriguing structural features, the unique binder-free Co_3O_4 hollow NPs/CNF hybrid film electrodes exhibit high specific capacitance (SC), excellent rate capability and cycling stability. As an example, the flexible hybrid film with loading of 35.9 wt% Co_3O_4 delivers a SC of 556 F g^{-1} at a current density of 1 A g^{-1}, and 403 F g^{-1} even at a very high current density of 12 A g^{-1}. Remarkably, almost no decay in SC is found after continuous charge/discharge cycling for 2000 cycles at 4 A g^{-1}. This exceptional electrochemical performance makes such novel self-supported Co_3O_4-CNFs hybrid films attractive for high-performance electrochemical capacitors.

1. Introduction

Recently, electrochemical capacitors (ECs) have sparked increasing attention as novel electric energy storage devices because they can provide an energy density higher by orders of magnitude than that of dielectric capacitors, and greater power density and longer cycling ability compared to conventional rechargeable batteries.[1–3] Particularly, amorphous hydrated RuO_2 has been recognized as the ideal electrode material for ECs, owing to its high proton and electron conductivity, large theoretical specific capacitance (SC) and good rate capability.[4,5] Nevertheless, the toxicity and high cost greatly prevent its large-scale use in ECs.[5] Thus, researchers worldwide are devoting tremendous amount of effort in exploring alternative economical electrode materials with excellent electrochemical performance for advanced ECs. Recent works have shown that some low-cost transition metal oxides (TMOs) (such as NiO, CoO_x, MnO_2, V_2O_5, etc.) also exhibit attractive supercapacitive behaviors.[6–9] Of particular note, Co_3O_4, which is widely available, relatively environmentally friendly and low-cost, has been extensively studied as a pseudocapacitive material for ECs, and considered as a promising alternative for the state-of-the-art RuO_2.[10–14] Unfortunately, like other simple TMOs, Co_3O_4 is a wide-bandgap semiconductor with poor electrical conductivity, which renders its low electrochemical utilization at high rates when used as the electroactive material for ECs. As a result, the reported SCs are far less than the theoretical SC value of about 3560 F g^{-1}. Also, unlike carbon materials, the cycling stability of Co_3O_4 is generally less satisfactory. It is therefore imperative and necessary to further boost its electrochemical performance by exploiting some efficient strategies to meet the requirement for practical use in ECs.

In general, upon reducing the dimension of electroactive Co_3O_4 to nanoscale, some attractive features benefiting efficient energy storage can be manifested.[2,7,10–12,15] However, the high surface energy commonly causes serious aggregation of nanosized Co_3O_4. In particular, the electroactive nanoparticles (NPs) are usually pelletized in a paste electrode for electrochemical evaluation. Thus, majority of the electrode surface is left behind as "inert surface" that cannot be accessed by electrolyte ions, resulting in insufficient Faradaic reactions for efficient energy storage.[11,12,15,16] Therefore, it would be more appealing if Co_3O_4 NPs, especially with a hollow feature, are highly dispersed upon and/or embedded in three-dimensional (3D) porous hierarchical supports with good electrical conductivity. This electrode design will on the one hand eliminate the tedious process of mixing and pressing electroactive materials with conducting additives and polymer binders, and at the same time provide a large bare surface accessible by electrolyte via the inherent porous diffusion channels and excellent electrical contact with the substrate. In other words, three fundamental prerequisites, including efficient ion diffusion, fast

Dr. F. Zhang, J. J. Zhu, J. Wang, Prof. X. G. Zhang
College of Material Science & Engineering
Nanjing University of Aeronautics and Astronautics
Nanjing, 210016, P. R. China
E-mail: azhangxg@163.com
Dr. C. Z. Yuan, Prof. X. W. Lou
School of Chemical and Biomedical Engineering
Nanyang Technological University
62 Nanyang Drive, Singapore 637459
E-mail: xwlou@ntu.edu.sg

DOI: 10.1002/adfm.201203844

electron transport and large amount of accessible electroactive sites, are simultaneously achieved by this electrode design for advanced high-performance ECs.[17–19]

Since the first exploration by Formhals,[20] electrospinning, as an industry-viable and versatile technique, has gained substantial attention in both academic research and industrial applications. With a post calcination treatment, it provides a straightforward and low-cost fabrication route to prepare 1D carbon nanofibers (CNFs),[21,22] and their derivatives with NPs (such as, SnO_2-CNFs, MoO_2-CNFs, MnO_2-CNFs).[23–25] More importantly, the collected 3D net-like CNF films possess many exciting characteristics, including large surface area to volume ratio, good mechanical strength, excellent flexibility, high porosity and desirable electrical conductivity,[21,22] which render such films a promising 3D support with hierarchical porosity for electroactive materials.

In this work, we report the interesting formation of Co_3O_4 hollow NPs in electrospun CNFs, and their derived 3D flexible porous Co_3O_4-CNFs hybrid films as intriguing self-supported electrodes for ECs. By simply tuning the relative amounts of polyacrylonitrile (PAN) and cobalt acetylacetonate ($Co(acac)_2$) in the precursor sol, Co_3O_4-CNFs hybrid porous films with loading of different amounts of electroactive Co_3O_4 can be obtained. Even when the PAN nanofibers (PNFs) are carbonized at a very high temperature to maximize the electrical conductivity of the final CNF matrix, Co_3O_4 hollow NPs are firmly adhered to the CNFs with good dispersion. The obtained unique binder-free Co_3O_4-CNFs hybrid films exhibit large SC, excellent rate capability and cycling stability, suggesting their promising applications in ECs.

2. Results and Discussion

The electrospinning strategy coupled with post annealing is applied to fabricate Co_3O_4 hollow NPs-CNFs, as illustrated in **Figure 1**. Specifically, the polymeric nanofibers containing cobalt precursor are first electrospun and further undergone thermal stabilization in air. After that, the cobalt salt is decomposed and reduced to metal Co NPs during carbonization in an inert atmosphere at a high temperature. The Co NPs

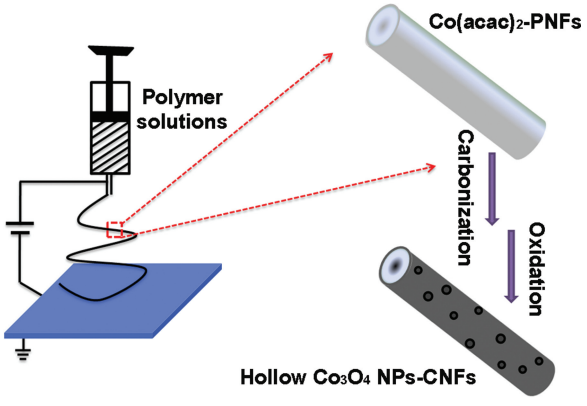

Figure 1. Schematic illustration of the preparation process of the hollow Co_3O_4 NPs-CNFs via an electrospinning and post annealing strategy.

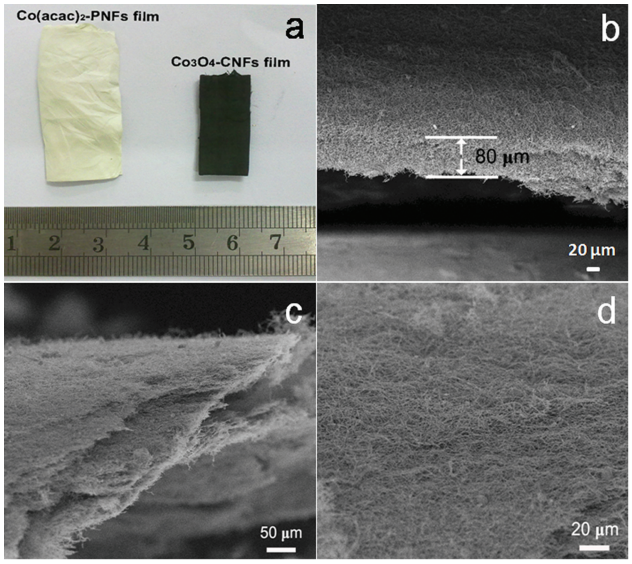

Figure 2. a) A digital photograph of the $Co(acac)_2$-PNFs and Co_3O_4-CNFs hybrid films. b,c) The side-view FESEM images and d) the top-view FESEM image of the Co_3O_4-CNFs hybrid films.

are subsequently oxidized in air to form Co_3O_4 hollow NPs attached to the CNFs. As seen in **Figure 2**a, the white electrospun $Co(acac)_2$-PAN nanofibers (denoted as $Co(acac)_2$-PNFs) mat-like film is evidently transformed into a black Co_3O_4-CNFs hybrid film with a smaller size owing to the shrinkage during annealing. Figure 2b,c show the field-emission scanning electron microscope (FESEM) images of the net-like Co_3O_4-CNFs hybrid film from the side view. The thickness of the hybrid fibrous mat film composed of multi-layers of folded nanofibers is about 80 μm. As seen from the top-view FESEM image of the hybrid film (Figure 2d), 3D porous cross-linked nanofiberous microstructures can be clearly observed.

The FESEM images of the electrospun $Co(acac)_2$-PNFs with various $Co(acac)_2$ loadings are shown in Figure S1 (Supporting Information). Evidently, 1D nanofiberous morphology with smooth surface and a uniform diameter of about 150 nm can be seen for the $Co(acac)_2$-PNFs1 sample (Figure S1a,b, Supporting Information) synthesized by adding 0.2 g of $Co(acac)_2$ in the polymer solution. When 0.3 g of $Co(acac)_2$ is introduced into the solution, the obtained $Co(acac)_2$-PNFs2 (Figure S1c,d, Supporting Information) still remains the 1D fiberous nanostructure with a larger fiber diameter of about 300 nm. When the amount of $Co(acac)_2$ is increased up to 0.5 g, some bulky "nodes" unexpectedly can be found in the obtained $Co(acac)_2$-PNFs3 sample (Figure S1e,f, Supporting Information). It is well known that the viscosity, ionic conductivity and surface tension of the polymer solution after addition of some metal salts would be altered, thus significantly affecting the morphologies of the resulting $Co(acac)_2$-PNFs samples.[26–29] As the concentration of $Co(acac)_2$ increases, the viscosity as well as surface tension of the PAN solution decreases, thus leading to the emergence of nodes due to the unstable efflux of the precursor solution in the electric field.

In order to obtain structurally integrated Co_3O_4-CNFs, a stepwise annealing strategy is applied to calcine the $Co(acac)_2$-PNFs

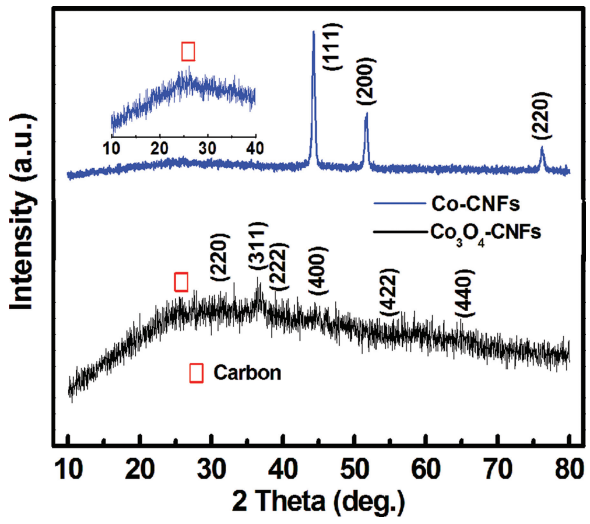

Figure 3. XRD patterns of Co-CNFs and Co_3O_4-CNFs films.

precursor films. First, the electrospun precursor films are held in air at 220 °C for 1.5 h, and the color of nanofiberous films changes to yellow from white. This step stabilizes the nanofiberous morphology. During the annealing, the PAN macromolecules in the as-electrospun nanofibers absorb oxygen in the air and undergo chemical changes, which result in the cyclization of PAN macromolecules and lead to formation of a stiff ladder-like polymeric structure that does not melt.[30] Thus, the 1D fiberous morphology can be retained during the subsequent carbonization process. By the thermogravimetric and differential scanning calorimetry (TG-DSC) analysis (Figure S2, Supporting Information) of $Co(acac)_2$ in N_2 atmosphere, two endothermic peaks around 220 °C and 350 °C can be observed, corresponding to the two steps of decomposition of $Co(acac)_2$. Then, the pretreated nanofiber film is further kept at 350 °C for 5 h in a N_2 atmosphere to ensure the complete decomposition. After the following annealing at 800 °C, the PNFs are transformed into 1D nanofiberous carbon framework with perfect structural integrity and good electrical conductivity. Simultaneously, the $Co(acac)_2$ precursor is completely reduced to Co species to form Co-CNFs hybrid films. Lastly, a mild oxidization annealing at 300 °C in air for only 20 min is further conducted to convert the Co species into Co_3O_4 hollow NPs.

To verify the crystalline structure of the as-synthesized Co_3O_4-CNFs films, typical powder X-ray diffraction (XRD) patterns are shown in **Figure 3**. After annealing in the N_2 atmosphere, three diffraction peaks at 2θ angles of about 44.2°, 51.5° and 75.8° are observed, which can be assigned to the (111), (200) and (220) reflections of the Co NPs (JCPDS card no. 15-0806). Another broad diffraction peak at 2θ of about 26° is indexed to the characteristic (002) reflection of amorphous carbon,[25] which is further verified by the Raman characterization (Figure S3, Supporting Information). This confirms that the $Co(acac)_2$-PNFs are decomposed and carbothermally reduced to Co-CNFs. In addition, the size of Co NPs is calculated to be about 20 nm by the Scherrer formula. Notably, after calcination at 300 °C in air, the diffraction peaks of Co NPs completely disappear, and some new diffraction peaks with low intensity are observed and indexed to the typical (220), (311), (222), (400), (422) and (440) reflections of the spinel Co_3O_4 (JCPDS card no. 42-1467). This suggests that the calcination in air for only 20 min is enough for the transformation of the elemental Co NPs into the Co_3O_4 phase.

The FESEM images of the as-synthesized Co_3O_4-CNFs with different Co_3O_4 loadings are shown in **Figure 4**. The Co_3O_4-CNFs1 preserves a similar 1D nanofiberous morphology (Figure 4a,b) compared to its precursor (i.e., $Co(acac)_2$-PNFs1). After careful examination, some Co_3O_4 NPs dispersed on the surface of CNFs can be easily seen from the magnified FESEM image (the inset in Figure 4b). As for the Co_3O_4-CNFs2 sample, the 1D fiberous nanostructure can also be well retained (Figure 4c,d). Of particular note, these Co_3O_4 NPs are not only dispersed uniformly on the surface of the CNFs, but also embedded into the CNF framework (see the region indicated by the circle) as evident in Figure 4e. Figure 4f shows the FESEM image of the Co_3O_4-CNFs3 sample, from which a few

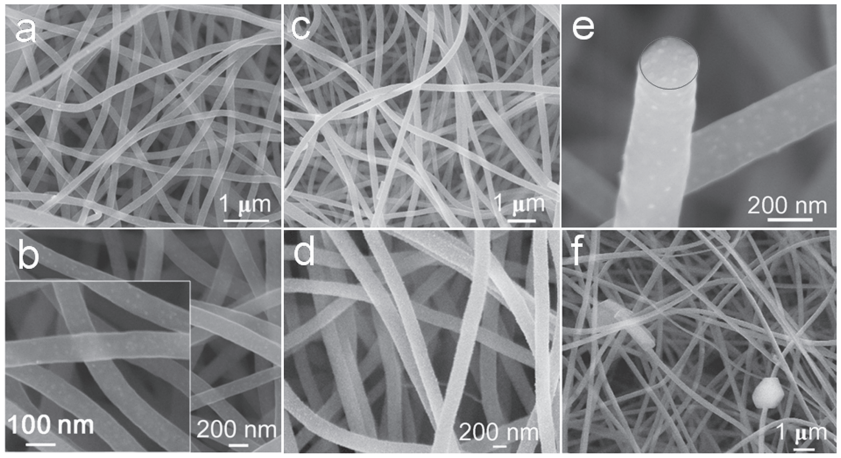

Figure 4. FESEM images of a,b) Co_3O_4-CNFs1, c–e) Co_3O_4-CNFs2, and f) Co_3O_4-CNFs3.

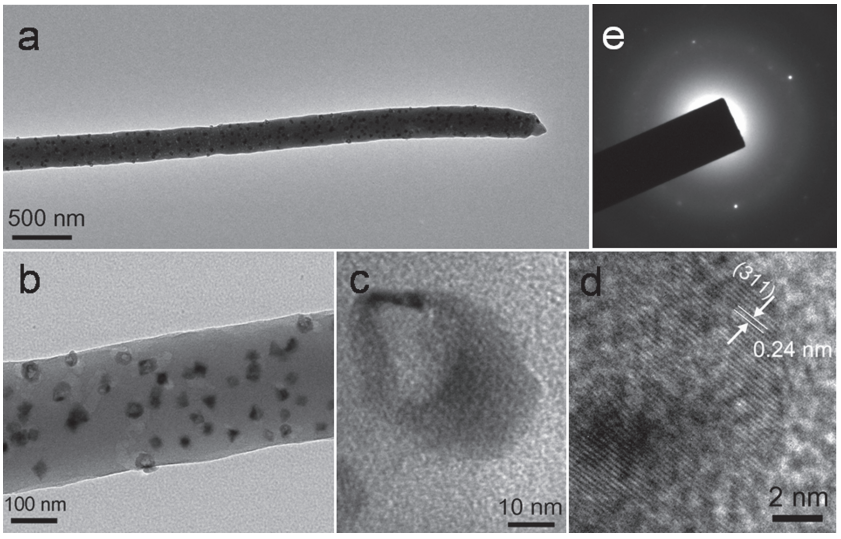

Figure 5. a,b) TEM images of a single nanofiber from the Co_3O_4-CNFs2 sample, c,d) HRTEM images of a single Co_3O_4 hollow NP, and e) the corresponding SAED pattern.

bulky nodes can be found by annealing its precursor Co(acac)$_2$-PNFs3. The chemical analysis by energy-dispersive X-ray spectroscopy (EDS) for the nodes region (Figure S4, Supporting Information) shows signals of C, O and Co elements. The C species possesses the highest intensity, and the Co and O signals further prove existence of the Co_3O_4 phase in these nodes. Based on the thermogravimetric analysis (TGA) data (Figure S5, Supporting Information), the mass loadings of Co_3O_4 in the Co_3O_4-CNFs1, Co_3O_4-CNFs2 and Co_3O_4-CNFs3 are 15.6 wt%, 21.7 wt% and 35.9 wt%, respectively. Besides the perfect morphological conservation mentioned above, it is found that the diameters of all the Co_3O_4-CNFs samples decrease compared to those of their corresponding Co(acac)$_2$-PNFs precursors. This is caused by the decomposition of the precursor during calcination,[31] which is also responsible for the size reduction of the Co(acac)$_2$-PNFs film after calcination as shown in Figure 2a.

Transmission electron microscopy (TEM) is employed to further characterize the microstructure of the hybrid Co_3O_4-CNFs. A typical TEM image of a single nanofiber from the Co_3O_4-CNFs2 sample is presented in **Figure 5**a,b. Clearly, the surface of the Co_3O_4-CNF is generally smooth with lots of Co_3O_4 NPs distributed uniformly on the surface and/or embedded in the CNF framework. Interestingly, it is observed that these Co_3O_4 NPs with a size ranged from 20 to 40 nm possess off-center hollow voids as shown in Figure 5b,c. The formation of hollow NPs can be easily understood and explained by the well-known Kirkendall effect during the transformation from Co NPs into Co_3O_4 hollow NPs.[32–34] When metal NPs are exposed in the oxygen-, sulfur- or phosphorus-rich environment, hollow NPs can be easily formed.[32] This is because that the speed of the outward diffusion of the cations is higher than that of the inward diffusion of the anions, which leads to the formation of hollow voids. After complete oxidation of the Co NPs, the Co_3O_4 shell is thinnest adjacent to the point where the hollow void nucleates and remains the same thickness. On the contrary, the Co_3O_4 shell is thickest opposite of the void because that the Co diffuses away from the void as it is oxidized. Thus, Co_3O_4 hollow NPs with nonuniform shell thickness are formed as observed in Figure 5c. A similar phenomenon is also observed during the oxidization of Ni NPs into NiO hollow NPs.[32] The high-resolution (HR) TEM image (Figure 5d) of the Co_3O_4 hollow NPs shell reveals well-resolved lattice fringes with an interplane distance of 0.24 nm, which corresponds to typical (311) crystal planes of the spinel Co_3O_4. The selected-area electron diffraction (SAED) pattern (Figure 5e) from a single NP demonstrates a polycrystalline structure of the Co_3O_4 hollow NPs. Interestingly, another distinct morphology is observed (Figure S6, Supporting Information) when the calcination time in air is prolonged to 40 min. Apparently, the 1D carbon framework is seriously damaged and the formed Co_3O_4 hollow NPs further fuse to form an aggregated solid structure. This clearly indicates the critical role played by the oxidation time in air in preserving the 1D uniform CNFs matrix and the hollow nature of Co_3O_4 NPs. It is also important to mention that the present synthesis strategy can be extended to fabricate NiO hollow nanocubes/CNFs hybrid nanostructures. As seen from TEM images (Figure S7a,b, Supporting Information), many hollow box-like NiO nanocubes of 15 nm in size are dispersed uniformly in the CNFs with a diameter of about 350 nm.

We next carry out electrochemical evaluation of these self-supported porous films made of Co_3O_4-CNFs as integrated electrodes for ECs. **Figure 6**a–c show the typical cyclic voltammetry (CV) curves of the three samples at various scan rates between 5 and 20 mV s^{-1} within the potential range of 0–0.5 V (vs. SCE). Clearly, typical redox peaks can be observed in the CV curves and the corresponding Faradaic reactions can be described as follows:

$$Co_3O_4 + OH^- + H_2O \leftrightarrow 3CoOOH + e^- \quad (1)$$

$$CoOOH + OH^- \leftrightarrow CoO_2 + H_2O + e^- \quad (2)$$

The anodic peak voltages for the above redox reactions are very close to each other, similar to those reported before,[35–37] hence only one anodic peak for the Faradaic oxidation reactions of Co^{2+}/Co^{3+} (Equation (1)) and Co^{3+}/Co^{4+} (Equation (2)) can be observed. And the two observed cathodic peaks are ascribed to their corresponding reduction processes. In addition, with the increasing scan rate, the electrochemical response current increases, while the CV shape almost keeps the same with slight shift of the peak position, indicating the good electrochemical reversibility and high rate performance of these three self-supported porous hybrid electrodes. To quantify the SC of these binder-free porous hybrid films, chronopotentiometry (CP) tests at various mass-normalized current densities ranged from 1 to 12 A g^{-1} are carried out within an electrochemical voltage window of 0.5 V (vs. SCE). Typical discharge curves are depicted in Figure 6d–f. Evidently, the existence of plateaus in the discharge curves suggests the typical

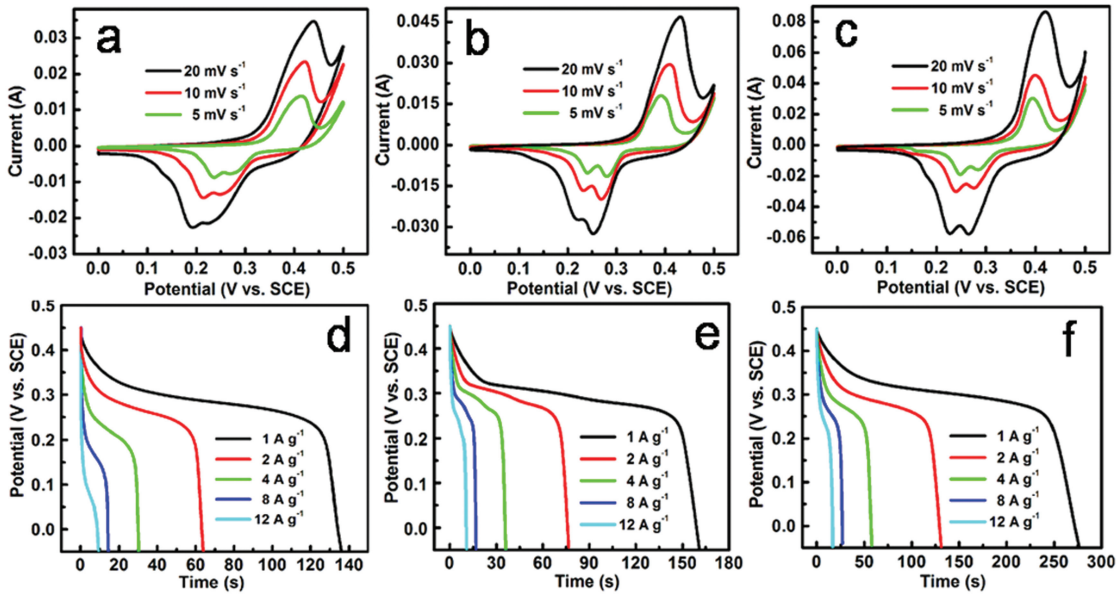

Figure 6. a–c) CV curves and d–f) discharge voltage profiles of Co_3O_4-CNFs1 (a,d), Co_3O_4-CNFs2 (b,e) and Co_3O_4-CNFs3 (c,f) film electrodes in 6 M KOH aqueous solution.

pseudocapacitive characteristics, which is in good agreement with the CV curves (Figure 6a–c). The SC of the three Co_3O_4-CNFs porous hybrid film electrodes is calculated and presented in **Figure 7**. Impressively, the Co_3O_4-CNFs3 hybrid film electrode exhibits the highest discharge SC of 552 F g^{-1} at 1 A g^{-1}. This should be related to its highest Co_3O_4 loading (Figure S5, Supporting Information). For the Co_3O_4-CNFs1 and Co_3O_4-CNFs2 electrodes, about 270 and 325 F g^{-1} can be delivered, respectively. It is important to point out that such electrospun carbon nanofibers show little electrochemical activity (≈26 F g^{-1} at 1 A g^{-1}, and 13 F g^{-1} at 8 A g^{-1}) in KOH aqueous solution in the voltage range of 0–0.5 V (vs. SCE), as shown in Figure S8 (Supporting Information).[38,39] Therefore, the SC of the Co_3O_4-CNFs hybrid films should be mainly contributed to by the Co_3O_4 phase. Taking into account the mass loadings of Co_3O_4 in the self-supported hybrid films, the pseudocapacitance of ≈1590, 1404 and 1491 F g^{-1} can be delivered by the electroactive Co_3O_4 at 1 A g^{-1} in Co_3O_4-CNFs1, Co_3O_4-CNFs2 and Co_3O_4-CNFs3, respectively. This reveals high electrochemical utilization of the electroactive Co_3O_4 hollow NPs in the self-supported hybrid porous film electrodes. The Co_3O_4-CNFs3 electrode exhibits not only high SC values but also excellent rate capability at higher current densities. Specifically, it delivers remarkable pseudocapacitance of 524, 462, 432 and 403 F g^{-1} at current densities of 2, 4, 8 and 12 A g^{-1}, respectively. This suggests that about 72% of the SC at 1 A g^{-1} is still retained when the discharge current density is increased to 12 A g^{-1}. For the same increase in current density from 1 to 12 A g^{-1}, the SC retention is even better for Co_3O_4-CNFs1 and Co_3O_4-CNFs2 because of their relatively low loading of Co_3O_4, namely about 83% (from 270 to 225 F g^{-1}) and 79% (from 325 to 256 F g^{-1}), respectively.

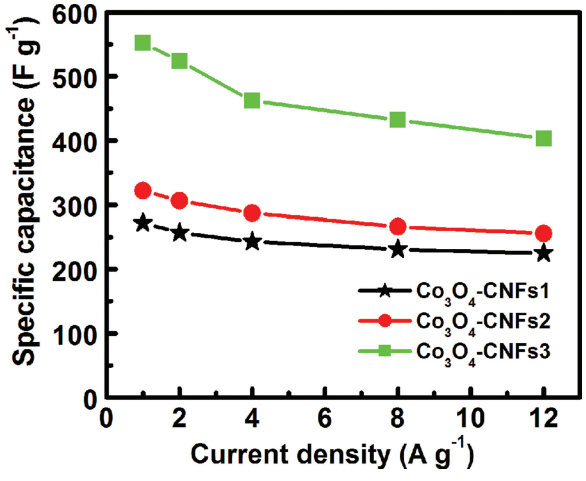

Figure 7. Specific capacitance of Co_3O_4-CNFs1, Co_3O_4-CNFs2 and Co_3O_4-CNFs3 film electrodes as a function of current density.

Figure 8 shows the cycling performance of the Co_3O_4-CNFs3 hybrid film electrode in 6 M KOH at a high current density of 4 A g^{-1} for 2000 cycles. In the course of the first 300 cycles, the SC of the self-supported hybrid porous film electrode gradually increases to about 484 F g^{-1}, which may result from the gradual activation process of the electroactive Co_3O_4 hollow NPs. Thereafter the SC is perfectly retained even after 2000 cycles with a negligible SC decay of about 1%, demonstrating its remarkable electrochemical stability. Also shown in Figure 8, the Coulombic efficiency of the Co_3O_4-CNFs3 electrode remains above 96% over the extended charge-discharge cycles. The enhanced compatibility and strong adhesion between these well-dispersed and stabilized fine Co_3O_4 hollow NPs and the 3D conductive CNFs should be responsible for the perfect retention of SC and excellent electrochemical stability during the continuous

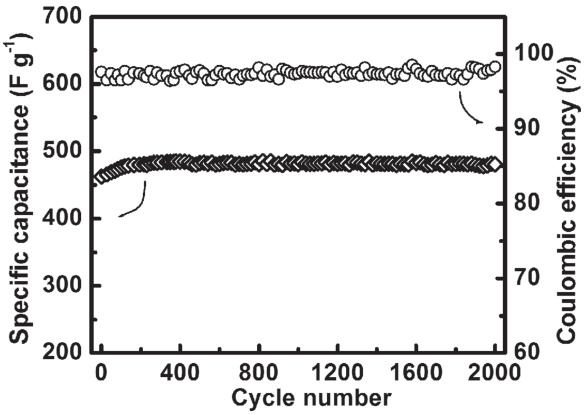

Figure 8. Cycling performance and Coulombic efficiency of the Co_3O_4-CNFs3 film electrode at a current density of 4 A g^{-1}.

cycling under a high-power density operation, as verified by the electrochemical impedance spectroscopy (ESI) characterization (Figure S9, Supporting Information). The overall electrochemical performance of the Co_3O_4-CNFs3 electrode in the present work is compared with that of many other carbon-Co_3O_4 hybrid electrodes previously reported (Table S1, Supporting Information), which shows the superiority of the former.

The above results evidently suggest that it is appealing to use such 3D hierarchical porous Co_3O_4-CNFs hybrid films as self-supported electrodes for advanced high-performance ECs. Their prominent ability to deliver high SC even at high charge-discharge current densities might be attributed to the attractive structural features of such binder-free film electrodes. Specifically, the hollow nature of the Co_3O_4 NPs embedded in the CNFs provides numerous electroactive sites for efficient Faradaic redox reactions. Also, the electrospun Co_3O_4 hollow NPs-CNFs hybrid films possess inherent 3D interconnected hierarchical porous structures, which serve as a robust reservoir for ions, ensure efficient contact between the surface of electroactive Co_3O_4 NPs and the electrolyte even at high rates, and hence significantly enhance the diffusion kinetics within the electrode. Furthermore, the direct integration of each Co_3O_4 hollow NP with the underneath CNFs "conductive network" builds up an express path for ultrafast electron transport, and thus avoids the use of additional polymer binder and conductive additives which commonly introduce extra contact resistance.

3. Conclusions

In summary, we have successfully developed an efficient electrospinning together with post stepwise annealing strategy for the controllable fabrication of carbon nanofibers incorporated with Co_3O_4 hollow nanoparticles. The collected Co_3O_4-CNF hybrid flexible mat-like films with tunable Co_3O_4 loadings are directly applied as integrated binder-free electrodes for high-performance electrochemical capacitors. The Co_3O_4 hollow nanoparticles are well dispersed in the conductive CNFs. Thanks to these advantageous structural features, the unique self-supported Co_3O_4-CNFs hybrid porous film electrodes manifest high specific capacitance and remarkable cycling stability at high current densities. The synthesis strategy is also successfully applied to incorporate NiO hollow nanoparticles in CNFs. It is therefore envisioned that the electrode design concept presented here can be easily generalized to incorporate other electroactive metal oxides and even mixed metal oxides to fabricate advanced binder-free electrodes for high-performance ECs and even Li-ion batteries.

4. Experimental Section

Synthesis of Co_3O_4 Hollow Nanoparticles/Carbon Nanofiber Hybrid Films: All the chemicals were of analytical grade and used as received without further purification. Typically, 0.8 g of polyacrylonitrile (PAN) was dissolved in 10 mL of N, N-dimethylformamide (DMF), and then 0.20 g of cobalt acetylacetonate ($Co(acac)_2$) was added to form a mixed solution. After vigorous stirring for 48 h at 60 °C, a red and sticky sol was obtained for the subsequent electrospinning process. In a typical electrospinning process, the precursor sol was loaded into a plastic syringe equipped with an N7-gauge needle made of stainless steel. The needle was connected to a 10 kV applied voltage and the distance between the needle tip and the collector was around 15 cm. A flow rate of 0.3 mL h^{-1} was employed. The as-electrospun $Co(acac)_2$/PAN nanofibers (denoted as $Co(acac)_2$-PNFs1) were dried for 24 h in vacuum at 60 °C. The dried $Co(acac)_2$-PNFs were further annealed in air at 220 °C for 1.5 h with a heating rate of 5 °C min^{-1}, then annealed in a N_2 flow at 350 °C for 5 h, and finally heated up to 800 °C for 1 h with a heating rate of 1 °C min^{-1}. The annealed product was designated as Co-CNFs. Finally, the as-made Co-CNFs sample was transformed into the Co_3O_4-CNFs via an oxidation process in air at 300 °C for 20 min. The final sample was denoted as Co_3O_4-CNFs1. The NiO-CNFs sample was synthesized in a similar method using $Ni(acac)_2$ as the metal source. For comparison, another three samples labelled as Co_3O_4-CNFs2, Co_3O_4-CNFs3 and CNFs were prepared by using 0.30, 0.50 and 0.0 g of $Co(acac)_2$ in the precursor sol, respectively, while all other conditions remained the same. The precursors for the Co_3O_4-CNFs2 and Co_3O_4-CNFs3 are denoted as $Co(acac)_2$-PNFs2 and $Co(acac)_2$-PNFs3, respectively. The conversion yield of PAN to carbon is about 40%.

Materials Characterization: The crystallographic phases of as-prepared samples were investigated using powder X-ray diffraction (XRD, Bruker D8 with Kα source) with a scanning rate of 3° min^{-1}. The morphologies and structures of the samples were examined by field-emission scanning electron microscope (FESEM, LEO, 1430VP, Germany), high-resolution transmission electron microscope (HRTEM), selected-area electron diffraction (SAED, FEI, TECNAI-20) and Raman spectroscopy (JY HR800, Tianjin). Thermogravimetric analysis (TGA, NETZSCH STA 409) measurements were carried out at a heating rate 10 °C min^{-1}.

Electrochemical Measurements: The Co_3O_4-CNFs films (1–1.2 mg cm^{-2}) were directly used as the working electrode for the following electrochemical tests by cyclic voltammetry (CV), chronopotentiometry (CP) and electrochemical impedance spectroscopy (EIS) on CHI660C electrochemical workstation (Chenhua, Shanghai). All measurements were carried out in a three-electrode cell with a working electrode, a platinum plate counter electrode and a saturated calomel electrode (SCE) as the reference electrode at room temperature. The electrolyte was a 6 M KOH aqueous solution. The cycling performance test was carried out with a CT2001D tester (Wuhan, China). The specific capacitance of these self-supported Co_3O_4-CNFs porous hybrid films can be calculated by using the following equation:

$$C_s = \frac{It}{m\Delta V} \quad (3)$$

where C_s is the specific capacitance (F g^{-1}) of these self-supported film electrodes, I is the discharge current density (A g^{-1}), t is the discharging

time (s), and ΔV is the discharge potential interval (V). Also, the SCs of Co_3O_4 can be obtained according to the following equation:[40]

$$C_{Co_3O_4} = \frac{C_{Co_3O_4-CNFs} - (1 - w_{Co_3O_4})C_{CNFs}}{w_{Co_3O_4}} \quad (4)$$

where $C_{Co_3O_4-CNFs}$, $C_{Co_3O_4}$, $w_{Co_3O_4}$, C_{CNFs} are the SCs of Co_3O_4-CNFs, and Co_3O_4 in the Co_3O_4-CNFs, the weight percentage of Co_3O_4 in the hybrid film and the SC of the CNFs, respectively.

Supporting Information

Supporting Information is available from the Wiley Online Library or from the author.

Acknowledgements

This work was partly supported by the National Natural Science Foundation of China (no. 21173120), and Nature Science Foundation of Jiangsu Province (no. BK2011030)

Received: December 26, 2012
Revised: February 10, 2013
Published online: March 26, 2013

[1] P. Simon, Y. Gogotsi, *Nat. Mater.* **2008**, *7*, 845.
[2] A. S. Arico, P. Bruce, B. Scrosati, J. M. Tarascon, W. V. Schalkwijk, *Nat. Mater.* **2005**, *4*, 366.
[3] R. B. Rakhi, W. Chen, D. Cha, H. N. Alshareef, *Nano Lett.* **2012**, *12*, 2559.
[4] Z. S. Wu, D. W. Wang, W. Ren, J. Zhao, G. Zhou, F. Li, H. M. Cheng, *Adv. Funct. Mater.* **2010**, *20*, 3595.
[5] R. R. Bi, X. L Wu, F. F. Cao, L. Y. Jiang, Y. G. Guo, L. J. Wan, *J. Phys. Chem. C* **2010**, *114*, 2448.
[6] C. Z. Yuan, X. G. Zhang, L. H. Su, B. Gao, L. F. Shen, *J. Mater. Chem.* **2009**, *19*, 5772.
[7] T. Zhu, J. S. Chen, X. W. Lou, *J. Mater. Chem.* **2010**, *20*, 7015.
[8] Y. H. Lin, T. Y. Wei, H. C. Chien, S. Y. Lu, *Adv. Energy Mater.* **2011**, *1*, 901.
[9] Z. Chen, V. Augustyn, J. Wen, Y. Zhang, M. Shen, B. Dunn, Y. Lu, *Adv. Mater.* **2011**, *23*, 791.
[10] C. Z. Yuan, L. Yang, L. R. Hou, J. Y. Li, Y. X. Sun, X. G. Zhang, L. F. Shen, X. J. Lu, S. L. Xiong, X. W. Lou, *Adv. Funct. Mater.* **2012**, *22*, 2560.
[11] F. Zhang, C. Z. Yuan, X. J. Lu, L. J. Zhang, Q. Che, X. G. Zhang, *J. Power Sources* **2012**, *203*, 250.
[12] X. H. Xia, J. P. Tu, X. L Wang, C. D. Gu, X. B. Zhao, *Chem. Commum.* **2011**, *47*, 5786.
[13] Y. Wang, Z. Zhong, Y. Chen, C. Ng, J. Lin, *Nano Res.* **2011**, *4*, 695.
[14] M. B. Zheng, J. Cao, S. T. Liao, J. S. Liu; H. Q. Chen, Y. Zhao, W. J. Dai, G. B. Ji, J. M. Cao, J. Tao, *J. Phys. Chem. C* **2009**, *113*, 3887.
[15] C. Z. Yuan, L. Yang, L. R. Hou, L. F. Shen, X. G. Zhang, X. W. Lou, *Energy Environ. Sci.* **2012**, *5*, 7883.
[16] C. Z. Yuan, L. Yang, L. R. Hou, L. F. Shen, F. Zhang, D. K. Li, X. G. Zhang, *J. Mater. Chem.* **2011**, *21*, 18183.
[17] T. Yu, Y. W. Zhu, X. J. Xu, Z. X. Shen, P. Chen, C. T. Lim, J. T. L. Thong, C. H. Sow, *Adv. Mater.* **2005**, *17*, 1595.
[18] J. Jiang, Y. Y. Li, J. P. Liu, X. T. Huang, C. Z. Yuan, X. W. Lou, *Adv. Mater.* **2012**, *24*, 5166.
[19] C. Z. Yuan, B. Gao, L. F. Shen, S. D. Yang, L. Hao, X. J. Lu, F. Zhang, L. J. Zhang, X. G. Zhang, *Nanoscale* **2011**, *3*, 529.
[20] Z. M. Huang, Y. Z. Zhang, M. Kotaki, *Compos. Sci. Technol.* **2003**, *63*, 2223.
[21] G. Wang, C. Pan, L. Wang, Q. Dong, C. Yu, Z. Zhao, J. S. Qiu, *Electrochim. Acta* **2012**, *69*, 65.
[22] G. Wang, Q. Dong, Z. Ling, C. Pan, C. Yu, J. S. Qiu, *J. Mater. Chem.* **2012**, *22*, 21819.
[23] C. A. Bonino, L. W. Ji, Z. Lin, X. W. Zhang, *ACS Appl. Mater. Interfaces* **2011**, *3*, 2534.
[24] W. Luo, X. L. Hu, Y. M. Sun, *Phys. Chem. Chem. Phys.* **2011**, *13*, 16735.
[25] K. N. Jung, J. I. Lee, S. Yoon, S. H. Yeon, W. Chang, K. H. Shin, J. W. Lee, *J. Mater. Chem.* **2012**, *22*, 21845.
[26] H. Fong, I. Chun, D. H. Reneker, *Polymer* **1999**, *40*, 4585.
[27] R. H. Magarvey, L. E. Outhouse, *J. Fluid Mech.* **1962**, *13*, 151.
[28] L. W. Ji, A. J. Medford, X. W. Zhang, *J. Polym. Sci. Part B: Polym. Phys.* **2009**, *47*, 493.
[29] L. W. Ji, Z. Lin, R. Zhou, Q. Shi, O. Toprakci, A. J. Medford, C. R. Millns, X. W. Zhang, *Electrochim. Acta* **2010**, *55*, 1605.
[30] Z. P. Zhou, C. L. Lai, L. F. Zhang, Y. Qian, H. Q. Hou, D. H. Reneker, H. Fong, *Polymer* **2009**, *50*, 2999.
[31] J. Mittal, O. P. Bahl, R. B. Mathur, *Carbon* **1997**, *35*, 1196.
[32] J. G. Railsback, A. C. Johnston-Peck, J. W. Wang, J. B. Tracy, *ACS Nano* **2010**, *4*, 1913.
[33] Y. Y. Liang, M. G. Schwab, L. J. Zhi, X. L. Feng, *J. Am. Chem. Soc.* **2010**, *132*, 15030.
[34] Y. D. Yin, R. M. Rioux, C. K. Erdonmez, Z. S. Hughes, G. A. Somorjai, A. P. Alivisatos, *Science* **2004**, *304*, 711.
[35] R. Tummala, R. K. Guduru, P. S. Mohanty, *J. Power Sources* **2012**, *209*, 44.
[36] J. P. Cheng, X. Chen, J. S. Wu, F. Liu, X. B. Zhang, V. P. Dravid, *CrystEngComm* **2012**, *14*, 6702.
[37] S. Huang, Y. Jin, M. Jia, *Electrochim. Acta* **2013**, *95*, 139.
[38] L. H. Su, X. G. Zhang, Y. Liu, *J. Solid State Electrochem.* **2008**, *12*, 1129.
[39] C. Z. Yuan, S. L. Xiong, X. G. Zhang, L. F. Shen, F. Zhang, B. Gao, L. H. Su, *Nano Res.* **2009**, *2*, 722.
[40] C. C. Hu, W. C. Chen, *Electrochim. Acta* **2004**, *49*, 3469.